AGU PUBLICATIONS

Geophysical Research Letters

RESEARCH LETTER
10.1002/2016GL067887

Key Points:
- A 65 year record of hourly Santa Ana Winds has been created
- ENSO and PDO modulate Santa Ana Winds intensity
- Santa Ana Winds increased in intensity with the 1970s PDO shift

Supporting Information:
- Supporting Information S1

Correspondence to:
J. Guzman-Morales,
jguzmanmorales@ucsd.edu

Citation:
Guzman-Morales, J., A. Gershunov, J. Theiss, H. Li, and D. Cayan (2016), Santa Ana Winds of Southern California: Their climatology, extremes, and behavior spanning six and a half decades, *Geophys. Res. Lett., 43*, 2827–2834, doi:10.1002/2016GL067887.

Received 27 JAN 2016
Accepted 9 MAR 2016
Accepted article online 14 MAR 2016
Published online 24 MAR 2016

Santa Ana Winds of Southern California: Their climatology, extremes, and behavior spanning six and a half decades

Janin Guzman-Morales[1], Alexander Gershunov[1], Jurgen Theiss[2], Haiqin Li[3,4], and Daniel Cayan[1,5]

[1]Scripps Institution of Oceanography, University of California, San Diego, La Jolla, California, USA, [2]Theiss Research, La Jolla, California, USA, [3]Cooperative Institute for Research in Environmental Science, University of Colorado Boulder, Boulder, Colorado, USA, [4]Earth System Research Laboratory, National Oceanic and Atmospheric Administration, Boulder, Colorado, USA, [5]United States Geological Survey, La Jolla, California, USA

Abstract Santa Ana Winds (SAWs) are an integral feature of the regional climate of Southern California/Northern Baja California region, but their climate-scale behavior is poorly understood. In the present work, we identify SAWs in mesoscale dynamical downscaling of a global reanalysis from 1948 to 2012. Model winds are validated with anemometer observations. SAWs exhibit an organized pattern with strongest easterly winds on westward facing downwind slopes and muted magnitudes at sea and over desert lowlands. We construct hourly local and regional SAW indices and analyze elements of their behavior on daily, annual, and multidecadal timescales. SAWs occurrences peak in winter, but some of the strongest winds have occurred in fall. Finally, we observe that SAW intensity is influenced by prominent large-scale low-frequency modes of climate variability rooted in the tropical and north Pacific ocean-atmosphere system.

1. Introduction

SAWs are episodic pulses of easterly, downslope, offshore flows over the coastal topography of the California Border Region (CBR): Southern California and Northern Baja California. SAWs represent a distinct and common regional cool season weather regime, a reversal of the typical wintertime onshore winds, contrasted with northwesterly alongshore and onshore flow characteristic of summer [*Conil and Hall*, 2006]. SAWs are associated with very dry air, often with anomalous warming at low elevations, and produce strong gusty downslope winds concentrated in gaps and on the lee slopes of the coastal ranges, e.g., Santa Ana, Santa Monica, and Laguna Mountains.

It is in these rugged hills and canyons, after long dry summers characteristic of this Mediterranean climate, that SAWs can drive catastrophic wildfires that CBR is infamous for [*Boyle*, 1995; *Moritz et al*., 2010; *Westerling et al*., 2004]. SAWs fanned the October 2007 wildfires that killed nine people, injured 85 others including 61 fire fighters, and destroyed upward of 1500 homes, scorching 2000 km^2 of land on the U.S. side of the border alone. The October 2003 SAW-fanned wildfires were even more extensive. Wind-blown smoke inhalation from these 2003 wildfires in Southern California resulted in 69 premature deaths, 778 hospitalizations, 1431 emergency room visits, and 47 K outpatient visits [*Delfino et al*., 2009]. More recently, the rare May 2014 events fanned extraordinarily late season fires following an extremely dry winter. Moreover, early and late season SAWs drive coastal heat waves, one reason why early fall rather than summer is historically the season for the hottest temperature extremes along the coast [*Gershunov and Guirguis*, 2012]. In spite of their tremendous episodic impacts on the health, economy, and mood of the region, a direct wind-based, long-term, and high-frequency climatology of SAWs is not available and relationships with larger-scale climate variability have not been clearly elucidated. This article begins to address these knowledge gaps for SAW behavior.

Indirect or proxy-based climatologies of SAWs have been typically diagnosed from synoptic-scale information. *Raphael* [2003] diagnosed 33 years of daily SAWs from observed pressure fields, while *Jones et al*. [2010] diagnosed 28 years of daily Fire Weather Index (FWI) [*Fosberg*, 1978] values, of which dry winds are a component, derived from the North American Regional Reanalysis [*Mesinger et al*., 2006]. *Abatzoglou et al*. [2013] developed the longest empirical daily reconstruction to date, from 1948 to 2012 based on pressure fields and temperature advection from global reanalysis.

Mesoscale modeling (MSM) has also been employed in the study of SAWs, typically to investigate the anatomy of SAWs from small samples of individual events [e.g., *Sommers*, 1978; *Lu et al*., 2012]. *Moritz et al*. [2010] provided a longer perspective using a decade of SAWs dynamically downscaled and demonstrated the ability

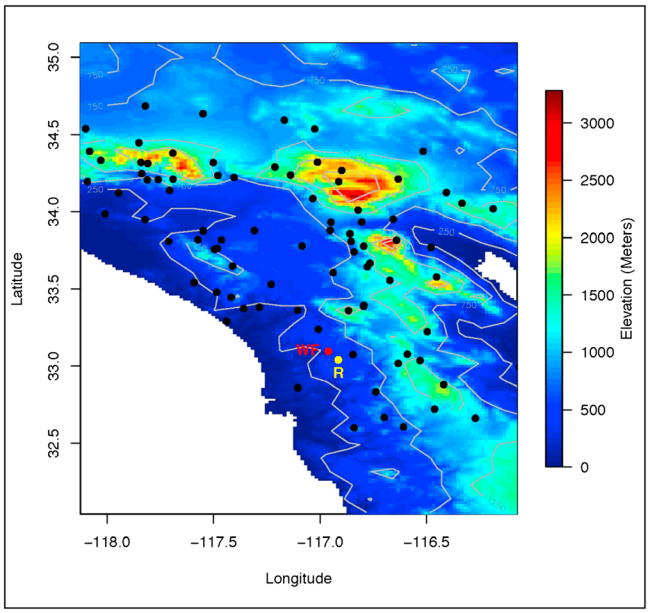

Figure 1. Spatial domain of the CBR with topography. Elevation is shown at 60 arc sec (colors) and 10 km spatial resolution (contours). Black dots mark the location of RAWS, and yellow dots show ASOS at Ramona Airport labeled "R." Location of Witch Creek Fire (WF) start in late October 2007 is shown as a red dot.

to predict large observed wildfire locations via model-derived FWI. Other studies have also employed MSM data sets spanning up to a decade with high spatiotemporal resolution to characterize SAWs among Southern California's regional weather regimes [*Conil and Hall*, 2006] and to investigate their causal mechanisms [*Hughes and Hall*, 2010]. Following on this work, *Hughes et al.* [2011] investigated anthropogenic climate change impacts on SAWs.

Here we use mesoscale modeling-derived wind data exclusively to define and quantify a long record of observationally validated SAWs. In what follows, we use observed wind to validate hourly winds in a 65 year dynamical downscaling of a global reanalysis to 10 km. We develop and apply a SAW definition with locally specific wind thresholds, and after determining their canonical spatial footprint, we define a SAW Domain, from which a SAW Regional Index is constructed. Subsequently, we examine the SAW climatology, paying particular attention to extremes, noteworthy events, interannual and longer-term variability. We finally discuss results in the context of regional climate variability, predictability and change, and in terms of their relevance to wildfire.

2. Data and Methods

2.1. Modeled Winds

To examine SAW variability in space and time, we use winds from the California Reanalysis Downscaling to 10 km, CaRD10 [*Kanamitsu and Kanamaru*, 2007]. CaRD10 provides hourly instantaneous winds at 10 m above the ground from 1948 to 2012, which is the longest mesoscale record to date. Our domain extends from (118.115°W, 35.081°N) at the NW point to (116.035°W, 32.053°N) at the most SE point with a total of 756 grid cells (21 × 36), capturing the core of the CBR extending 65 km across the border into Northern Baja California, Mexico (Figure 1).

2.2. Validation

The model skill is tested against sustained wind (wind speed average) and wind gust (maximum "instantaneous" wind speed) observations from 85 Remote Automated Weather Stations (RAWS) and one Automated Surface Observing System station (ASOS) across the domain (shown in Figure 1). Correlation coefficient (r) and normalized root mean squared error (NRMSE) are calculated for the overlapping part of the stations and CaRD10 records.

CaRD10 winds correlate more strongly with gusts than sustained winds at 78 (91% of) stations. This consistently stronger link with observed gusts is seen on the histograms shown in Figures S1a and S1b. Errors, measured as NRMSE, against gusts are also consistently smaller than errors against sustained winds (Figures S2a and S2b); this is the case at 65 (76% of) stations. When using SAWs (see section 2.3 for the definition of SAW) only, correlations at some stations improve but deteriorate at others (see flatter histograms in Figures S1c and S1d compared to Figures S1a and S1b). However, the agreement between modeled SAWs and observations still consistently favors observed gust over sustained wind (Figures S1c, S1d, S2c, and S2d). Modeled winds are instantaneous, neither sustained nor gust. Modeled winds overestimate sustained near-surface winds. Beyond possible model biases, part of the reason for this may be that observed winds are affected by fine-scale orography, as well as

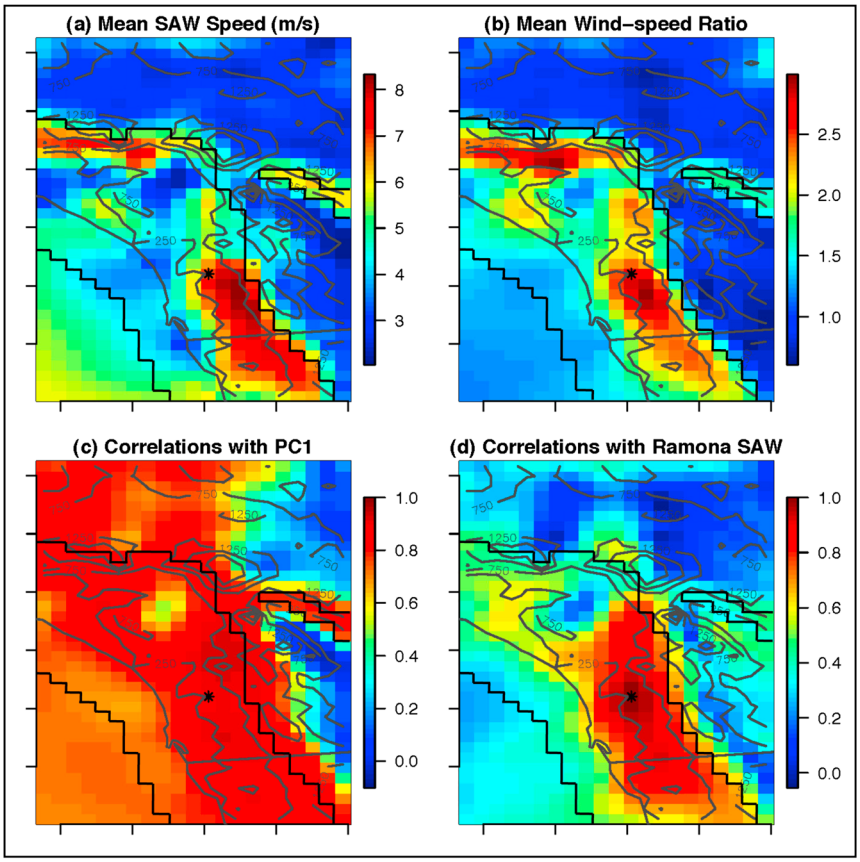

Figure 2. SAW spatial patterns. (a) Means, (b) ratios of SAW to all other winds, (c) correlations of local SAW time series with the leading SAW principal component (PC1), and (d) correlations of SAWRI time series with Ramona SAW. Black line marks SAW Domain on each map. All means and correlations are based on hourly data.

obstructions around the anemometer, not resolved by the model. Gusts are less sensitive to such features as they are more related to the flow above the boundary layer via turbulent mixing [*Brasseur*, 2001].

2.3. Local Definition of Santa Ana Winds

Modeled strong winds tend to converge between easterly and northeasterly directions with surface relative humidity dropping into single digits (Figure S3). This behavior suggests that wind direction and speed are sufficient to define SAWs. At each grid cell or station, we first identify winds with directions $>0°$ and $<180°$ (winds with a negative u component) and define local speed thresholds as the upper quartile of the direction-selected winds. Periods with at least 12 h of continuous selected winds that exceed the local wind speed threshold for at least 1 h are defined as SAWs. Discontinuities are allowed for periods of 12 h or less, to allow for breaks in SAW events, e.g., competing afternoon sea breeze episodes. The resulting SAW index reflects the full wind speed during periods that fulfill the direction-continuity scheme.

Ramona, California (Figure 1), located in west facing foothills of the Laguna Mountains, is known to be a windy fire prone location where the late October Cedar Fire (2003) and Witch Creek Fire (2007) burned during severe multiple wildfire episodes. In this work, we turn to Ramona for local examples. The correlation for the whole period of available gust and sustained wind observations (from 2005 to 2010) with Ramona SAW is 0.7 and 0.6, respectively. Figure S4b shows the excellent agreement between SAW and observed gust at Ramona, during early season SAW events of 2007 and 2010.

2.4. Regionalizing Local SAWs

We examine the spatial and seasonal coherence of locally defined SAWs. In the CaRD10 data set, the strongest SAWs are found on downwind slopes of the main topography, while SAWs relative to other winds reflect an almost identical pattern (Figures 2a and 2b) with comparatively lower values at sea, and lowest values over

the desert basins. This SAW speed spatial distribution is notably consistent with *Hughes and Hall* [2010] who determined it to be forced by katabatic acceleration of cool air downslope as well as downward momentum transfer.

We calculate the empirical orthogonal functions of hourly SAWs. The leading principal component (PC1) explains 50% of the total hourly SAWs variance over the region and its time series corresponds to SAW seasonality (Figure S5a). Broad regional coherence of SAW selection is displayed as correlations of PC1 with SAWs time series (Figure 2c). We also quantify the regional concurrence of SAWs across the domain with Ramona SAWs (Figure 2d), noting that SAWs at selected locations are well represented by the regional aggregate SAW index (described below).

Consistent with the above results, we define the SAW Domain as the region displaying coherent SAWs in time and magnitude. Thus, the SAW Domain is explicitly constrained to grid cells where PC1 explains 50% of the variance, i.e., where correlations between SAWs and PC1 exceed 0.7 and by high wind speed ratios (>1.5). For the sake of continuity, we include the low-ratio cluster of grid cells northeast of the Santa Ana Mountains and adjacent ocean grid cells (~40 km offshore). SAW Domain covers 43% of the original domain (Figure 2).

The SAW Regional Index (SAWRI) is then defined as the hourly average of the SAWs across all the grid cells within the SAW Domain. Hourly SAWRI is correlated with PC1 at $r = 0.9$ and with Ramona SAWs at $r = 0.7$. We reconstruct two seasons of observed SAW Regional Index ($SAWRI_{obs}$) from in situ wind observations. The correlation between the hourly SAWRI and $SAWRI_{obs}$ is 0.6. Comparison at different temporal resolutions is shown in Figure S5.

SAW events are directly quantified by continuous periods of SAWRI and classified into three categories according to their maximum SAWRI—weak ($<5\ m\ s^{-1}$), moderate ($5–10\ m\ s^{-1}$), and extreme ($10–15\ m\ s^{-1}$). Extremes events are above the 90th percentile of all events on record. Finally, we integrate SAWRI overtime to obtain total seasonal SAW intensity.

3. Results

3.1. SAW Climatology

Regionally, i.e., using SAWRI we detect a total of 2056 events on the 65 year record yielding an average of 32 occurrences per year. Typical SAW episodes last 1–2 days and represent 27% of the occurrences (Figure S6a). SAW events lasting up to 6 days account for 90% of all occurrences. The remaining 10% are made up almost entirely of events lasting between 7 and 12 days. Locally, the occurrence of events lasting 1–2 days is consistent with regional detection (also 27% of all events). However, shorter events (between 12 and 24 h) are the most frequent (Figure S6b). This suggests that mild SAW pulses over most active SAW locations (red areas in Figure 2a) may not be detected regionally, as they dissipate before reaching the coast. The mean and maximum SAWRI representing events lasting up to 5 days appear to increase linearly with duration (Figures S6c and S6e). For events longer than 5 days, the mean and maximum SAWRI reach limit speeds (~5 and $9\ m\ s^{-1}$, respectively) regardless of their duration. The duration-intensity relation for local SAWs is comparable (see Figures S6d and S6f) to regional results.

The SAW season extends from October to April, when SAW events occur at least twice per average month (Figure 3d). SAWs tend to be most frequent in December but most durable and strong in January. Early and late season SAW episodes occur, on average, about once per month in September and May, and typically exhibit moderate duration, and moderate regional speeds, i.e., mean and maximum SAWRI (Figures 3a–3c). Although not on our record, the two events of May 2014 (http://abcnews.go.com/topics/news/weather/santa-ana-winds.htm) appear to have been exceptional. This seasonal cycle of SAWs, although described in more detail here, generally agrees with seasonality identified in other studies [*Jones et al.*, 2010; *Raphael*, 2003].

In addition to the seasonal cycle, the hourly SAWRI resolves a well-defined diurnal cycle (Figure S7), reaching their maximum in the morning and decay to their minimum in the late afternoon. Local diurnal cycle of SAWs is line with SAWRI; however, inland and coastal locations are slightly different. At the coast, the onshore sea breeze may to some extent counteract SAWs starting in the morning and during some events the winds may reverse in the late afternoon.

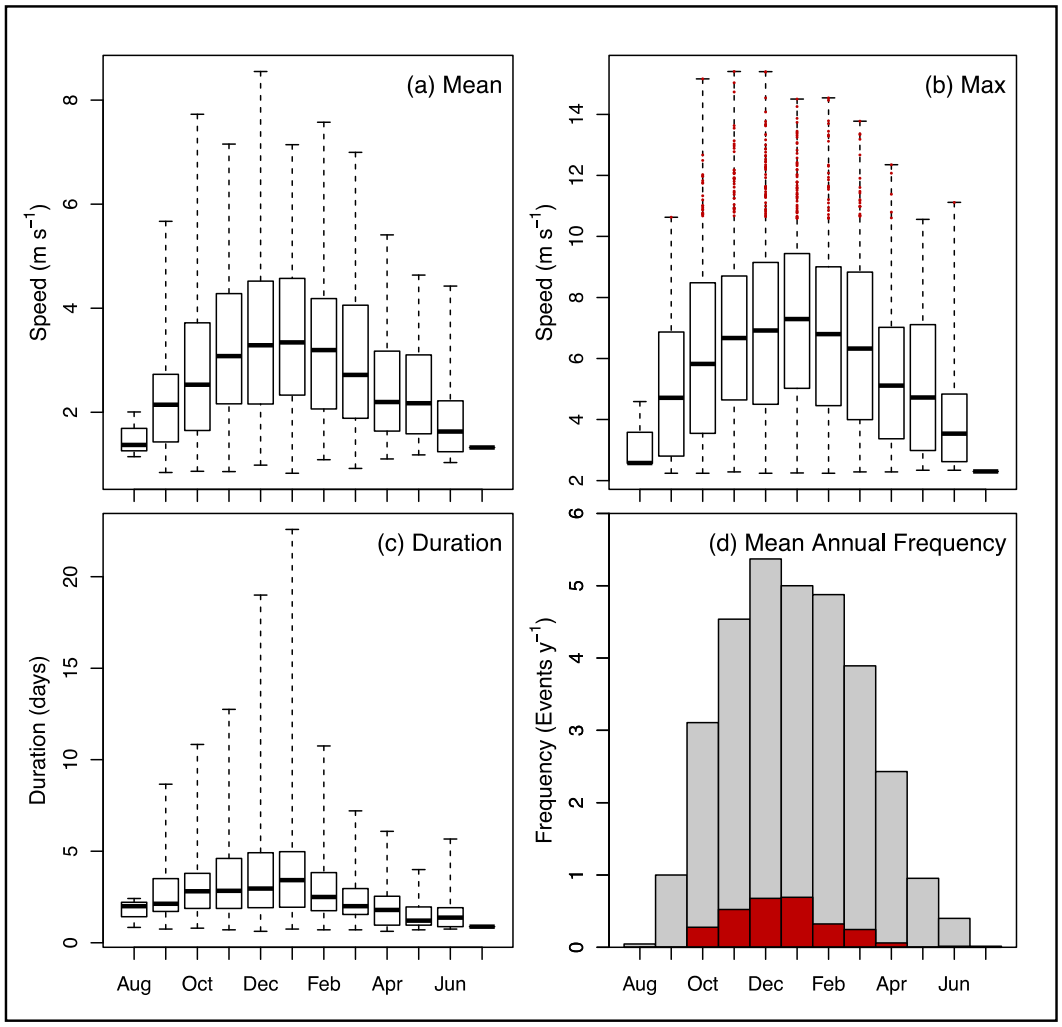

Figure 3. Climatology of regional SAW events (SAWRI). Monthly distribution of (a) mean SAWRI per event, (b) maximum SAWRI per event, (c) duration, and (d) mean monthly frequency per season of SAW events detected from 1948 to 2012. In Figures 3a–3c bold lines show median values, boxes delimit the first and third quartiles, and whiskers mark maximum and minimum values for each month. Extremes SAWs are shown in dark red in Figures 3b and 3d.

3.2. Climatology of SAW Extremes

Under the SAW and extreme definitions established, extremes account for 10% of the total number of events (on average three events per year). Extreme SAWs are most common in December, and January, but also occur in the shoulder seasons, with more extremes in fall compared to spring (red histogram in Figure 3d). Even though the highest frequency of extreme events is observed during the coldest months, maximum SAWRI can be just as extreme in the fall (Figure 3b). For example, three out of the top five SAW events with maximum SAWRI above 15 m s^{-1} occurred in fall.

3.3. Variability and Trends

Our results indicate considerable variability of SAW frequency, duration, and total intensity (total or by category) on interannual to decadal time scales. There are no significant long-term trends (Figures 4a–4c), except for a modest upward trend in the intensity of extreme SAWs (Figure 4d). For the record the frequency of extreme events accounts for 9% of all SAW events, but they contribute 25% to the total seasonal intensity. Closer examination reveals that this trend results mainly from a step-function-type change that roughly corresponds to the North Pacific climate shift in the mid-1970s [*Mantua and Hare*, 2002]. A similar shift is also evident in the SAW duration and intensity (Figures 4b and 4c). The shift in these other variables, although not resulting in a significant trend, is much more in line with the 1976 Pacific Decadal Oscillation (PDO) shift.

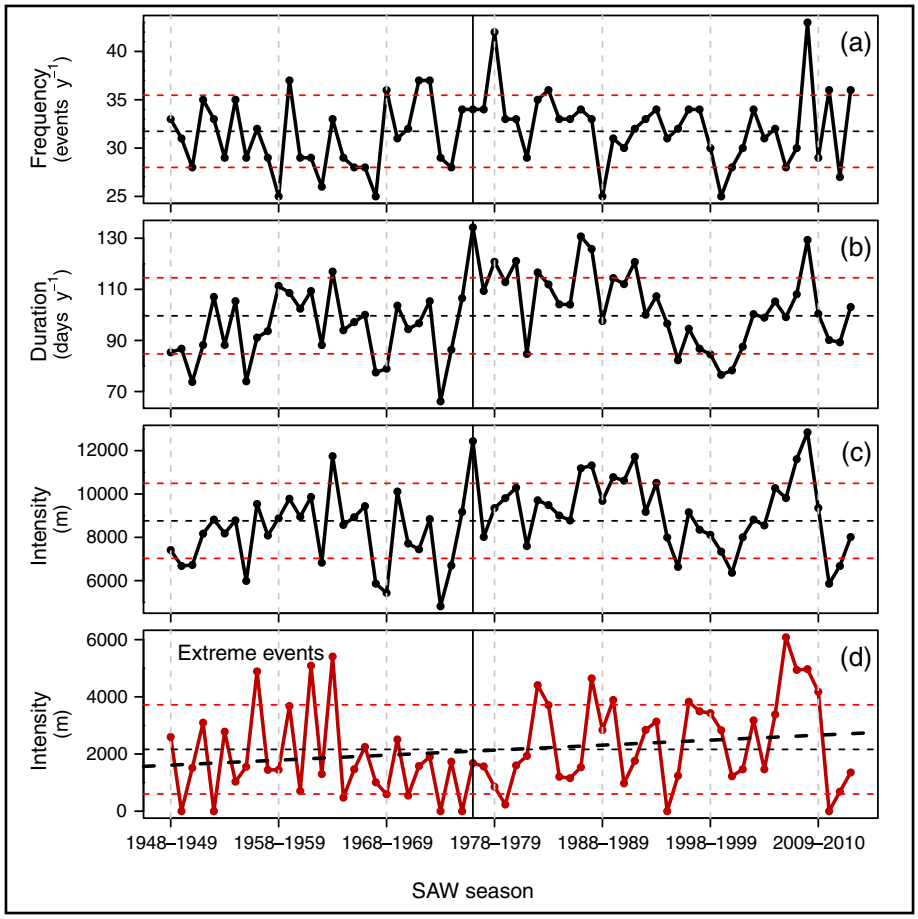

Figure 4. Seasonal (August–July) variability of total (a) frequency, (b) duration, (c) intensity, and (d) intensity of extreme events. The linear regression fits are shown only if significant. Solid black line marks the change of PDO to its positive phase in 1976.

3.4. Potential Seasonal Predictability

The time series in Figure 4 indicate a change in the behavior of seasonal SAW intensities coinciding with the shift of the Pacific Decadal Oscillation (PDO) to its positive phase in 1977. This suggests that seasonal atmospheric anomalies associated with PDO teleconnections [*Favre and Gershunov*, 2009; *Mantua and Hare*, 2002] may influence SAW activity. Because PDO teleconnections influence circulation anomalies via their modulation of El Niño–Southern Oscillation (ENSO) teleconnections [*Gershunov and Barnett*, 1998], we examine total seasonal SAW intensity anomalies composited by ENSO and PDO phases. Moreover, *Raphael* [2003] suggested a relationship between ENSO and late season (February–March) SAW frequency.

Intensity anomalies are shown in box-and-whisker plots spanning the composite samples and quantified in percent deviation from the 65 year SAWRI climatology (Figure 5). We use bootstrapping as in *Gershunov and Barnett* [1998] to test whether composite mean deviations from climatology are significant. We find a significant positive signal in El Niño/PDO(+) years amounting to ~10% increased intensity and a negative signal in La Niña/PDO(−) years amounting to ~10% decrease in regional SAW intensity. These are the same constructive ENSO/PDO interactions that account for predictable precipitation signals [*Gershunov and Barnett*, 1998] such that enhanced/decreased SAW activity tends to coincide with enhanced/decreased precipitation seasonally. This bodes well for seasonal fire danger, but obviously, there is a lot of scatter in the composites as is seen on Figure 5. The significant relationship we find between SAW and ENSO is broadly consistent with the suggestion of *Raphael* [2003] that El Niño is

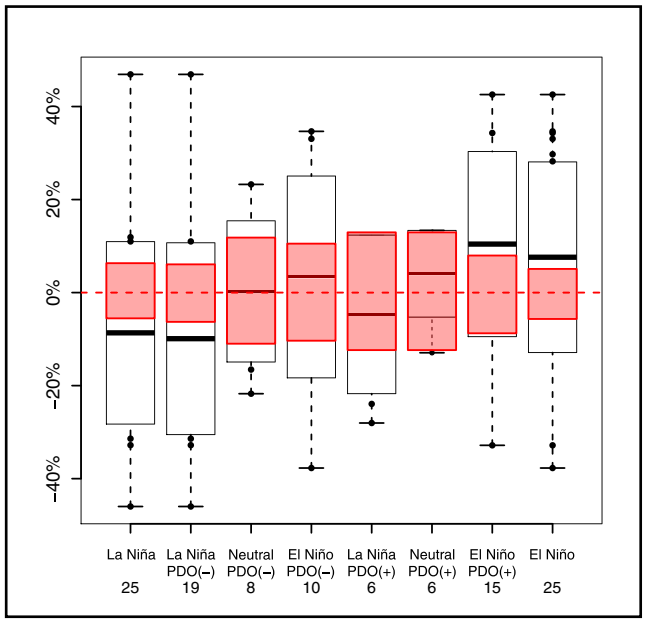

Figure 5. ENSO and ENSO-PDO joint composite anomaly of the integrated seasonal total SAWRI relative to the 65 year SAWRI climatology in percent. Numbers below each category are the number of SAW seasons (sample) that fell into the given composite. Boxes show one standard deviation from the mean, dots are outliers, and whisker marks the maximum and minimum outliers. Red boxes outline the 95% confidence region for means of bootstrapped (random) sampling distributions so that a sample mean lying outside the red zone signifies a statistically significant signal revealed with 95% confidence.

associated with longer SAW events, while contrary to *Berg et al.* [2013] who suggest the opposite association. It is worth noting that the relationship we find between seasonal SAW intensity and ENSO appears to be partly modulated by PDO.

4. Discussion and Conclusions

In this work, we present direct local and regional long-term perspectives on hourly Santa Ana Winds that address specific voids in current knowledge: (1) constructing a long-term, high-resolution, region-wide climatology against which the evolving SAW mean and extreme conditions in magnitude and time can be assessed and (2) validation using a broad network of wind observations to realistically address local and regional variability.

The seasonal frequency of SAW clearly reflects mechanisms responsible for peak SAW frequency in December and January. These months have the least sunshine and longest nights essential for producing cold air masses over the Great Basin—the necessary condition for SAW. These months also experience a peak in transient synoptic activity that causes strong pressure gradients—the triggers of SAWs. On average longer events shift to higher SAWRI means and maxima up to 6 days but with a wide dispersion for each duration bin. The weak relationship between duration of SAW events and their maximum speeds agrees well with the fact that some events are mostly associated with local temperature gradient, while others are synoptically driven. A combination of these forcing mechanisms produces strong and long-lasting SAWs [*Hughes and Hall*, 2010]. The cold air pooling over the elevated Great Basin also results in diurnal cycles of SAWs, which are strongest in the early morning hours when the thermodynamic mechanism is enhanced.

Under climate change, the Great Basin is projected to warm faster than the coastal region, which suggests that SAW occurrence may diminish [*Hughes et al.*, 2011]. However, the reconstructed historical record of SAWs does not thus far support such expectation. Instead, it raises new questions about future SAWs and fire seasons. The only long-term trend that we observe is in the extremes of SAWs, which appears to be related to the mid-1970s North Pacific climate shift.

We find that seasonal SAW intensity is sensitive to prominent large-scale low-frequency modes of climate variability rooted in the tropical and North Pacific ocean-atmosphere system. These same modes are also known to predictably affect the hydroclimate of this region [*Gershunov and Cayan*, 2003]. As is the case with regional seasonal precipitation anomalies, seasonal SAW intensity is enhanced during El Niño (especially if PDO is positive) and subdued during La Niña (especially if PDO is negative) winters. This SAW intensification during El Niño/PDO(+) seasons may be due to the southward displaced stormtrack and generally stronger synoptic activity enhancing the offshore pressure gradients that drive SAWs. Our empirical results suggest that seasonal ENSO-related prediction of SAW activity and fire risk may be possible, a topic for further investigation. These results taken together with the known sensitivity of regional hydroclimate to global climate change [*Polade et al.*, 2014], warrant a fresh look at climate change projections of SAWs, precipitation regime and fire risk.

Acknowledgments
We are grateful to CONACYT-UCMEXUS (http://ucmexus.ucr.edu/) for providing financial support to Janin Guzman-Morales (scholar 214550). We also appreciate support from Climate Education Partners, a National Science Foundation funded project DUE-1239797 (www.sandiego.edu/climate). This study also contributes to DOI's Southwest Climate Science Center activities and NOAA's California and Nevada Applications Program award NA11OAR43101. The derived gridded data of local SAWs as well as the SAWRI can be accessed at http://cnap.ucsd.edu/data/janin/.

References

Abatzoglou, J. T., R. Barbero, and N. J. Nauslar (2013), Diagnosing Santa Ana Winds in Southern California with synoptic-scale analysis, *Weather Forecast.*, *28*(3), 704–710.
Berg, N., et al. (2013), El Niño-Southern Oscillation impacts on winter winds over Southern California, *Clim. Dyn.*, *40*(1), 109–121.
Boyle, T. C. (1995), *The Tortilla Curtain*, 368 pp., Viking, New York.
Brasseur, O. (2001), Development and application of a physical approach to estimating wind gusts, *Mon. Weather Rev.*, *129*(1), 5–25.
Conil, S., and A. Hall (2006), Local regimes of atmospheric variability: A case study of Southern California, *J. Clim.*, *19*(17), 4308–4325.
Delfino, R. J., et al. (2009), The relationship of respiratory and cardiovascular hospital admissions to the Southern California wildfires of 2003, *Occup. Environ. Med.*, *66*(3), 189–197.
Favre, A., and A. Gershunov (2009), North Pacific cyclonic and anticyclonic transients in a global warming context: Possible consequences for Western North American daily precipitation and temperature extremes, *Clim. Dyn.*, *32*(7–8), 969–987.
Fosberg, M. A. (1978), Weather in wildland fire management—Fire weather index, *Bull. Am. Meteorol. Soc.*, *59*(3), 341.
Gershunov, A., and T. P. Barnett (1998), Interdecadal modulation of ENSO teleconnections, *Bull. Am. Meteorol. Soc.*, *79*(12), 2715–2725.
Gershunov, A., and D. R. Cayan (2003), Heavy daily precipitation frequency over the contiguous United States: Sources of climatic variability and seasonal predictability, *J. Clim.*, *16*(16), 2752–2765.
Gershunov, A., and K. Guirguis (2012), California heat waves in the present and future, *Geophys. Res. Lett.*, *39*, L18710, doi:10.1029/2012GL052979.
Hughes, M., and A. Hall (2010), Local and synoptic mechanisms causing Southern California's Santa Ana Winds, *Clim. Dyn.*, *34*(6), 847–857.
Hughes, M., A. Hall, and J. Kim (2011), Human-induced changes in wind, temperature and relative humidity during Santa Ana events, *Clim. Change*, *109*, 119–132.
Jones, C., F. Fujioka, and L. M. V. Carvalho (2010), Forecast skill of synoptic conditions associated with Santa Ana Winds in Southern California, *Mon. Weather Rev.*, *138*(12), 4528–4541.
Kanamitsu, M., and H. Kanamaru (2007), Fifty-seven-year California Reanalysis Downscaling at 10 km (CaRD10). Part I: System detail and validation with observations, *J. Clim.*, *20*(22), 5553–5571.
Lu, W., S. Zhong, J. J. Charney, X. Bian, and S. Liu (2012), WRF simulation over complex terrain during a southern California wildfire event, *J. Geophys. Res.*, *117*, D05125, doi:10.1029/2011JD017004.
Mantua, N. J., and S. R. Hare (2002), The Pacific decadal oscillation, *J. Oceanogr.*, *58*(1), 35–44.
Mesinger, F., et al. (2006), North American regional reanalysis, *Bull. Am. Meteorol. Soc.*, *87*(3), 343–360.
Moritz, M. A., T. J. Moody, M. A. Krawchuk, M. Hughes, and A. Hall (2010), Spatial variation in extreme winds predicts large wildfire locations in chaparral ecosystems, *Geophys. Res. Lett.*, *37*, L04801, doi:10.1029/2009GL041735.
Polade, S. D., D. W. Pierce, D. R. Cayan, A. Gershunov, and M. D. Dettinger (2014), The key role of dry days in changing regional climate and precipitation regimes, *Sci. Rep.*, *4*, 4364.
Raphael, M. N. (2003), The Santa Ana Winds of California, *Earth Interact.*, *7*, 1–13, doi:10.1175/1087-3562(2003)007<0001:TSAWOC>2.0.CO;2.
Sommers, W. T. (1978), LFM forecast variables related to Santa-Ana Wind occurrences, *Mon. Weather Rev.*, *106*(9), 1307–1316.
Westerling, A. L., D. R. Cayan, T. J. Brown, B. L. Hall, and L. G. Riddle (2004), Climate, Santa Ana Winds and autumn wildfires in Southern California, *Eos Trans. AGU*, *85*(31), 289–296, doi:10.1029/2004EO310001.